The Pion Single-Event Latch-Up Cross Section Enhancement: Mechanisms and Consequences for Accelerator Hardness Assurance

Andrea Coronetti, *Student Member, IEEE*, Rubén García Alía, *Member, IEEE*, Francesco Cerutti, Wojtek Hajdas, Daniel Söderström, *Student Member, IEEE*, Arto Javanainen, *Member, IEEE*, and Frédéric Saigné

***Abstract*— Pions make up a large part of the hadronic environment typical of accelerator mixed fields. Characterizing device cross sections against pions is usually disregarded in favor of tests with protons, whose single-event latch-up (SEL) cross section is, nonetheless, experimentally found to be lower than that of pions for all energies below 250 MeV. While Monte Carlo simulations are capable of reproducing such behavior, the reason for the observed pion cross-section enhancement can only be explained by a deeper analysis of the underlying mechanisms dominating proton–silicon and pion–silicon reactions. The mechanisms dominating the SEL response are found to vary with the energy under consideration. While a higher pion nuclear reaction rate, that is, probability of interaction, can explain the observed latch-up cross-section enhancement at energies >100 MeV, it is the volume-equivalent linear energy transfer (LET_{EQ}) of the secondary ions that keeps the pion latch-up response high at lower energies. The higher LET_{EQ} of secondary ions from pion–silicon interactions is caused by the pion absorption mechanism, which is highly exothermic. In spite of the observed higher cross section for pions, the high-energy hadron approximation is found to still provide reliable estimations of the latch-up response of a device in mixed fields.**

***Index Terms*— Accelerator, cross section, FLUKA, neutrons, nuclear interactions, pions, protons, radiation hardness assurance (RHA), single-event latch-up (SEL).**

Manuscript received February 9, 2021; revised March 24, 2021; accepted March 26, 2021. Date of publication March 31, 2021; date of current version August 16, 2021. This work was supported by the European Union's Horizon 2020 Research and Innovation Program through Marie Sklodowska Curie (MSC) under Grant 721624.

Andrea Coronetti is with CERN, 1211 Geneva, Switzerland, and also with the Department of Physics, University of Jyväskylä, 40014 Jyväskylä, Finland (e-mail: andrea.coronetti@cern.ch).

Rubén García Alía and Francesco Cerutti are with CERN, 1211 Geneva, Switzerland.

Wojtek Hajdas is with the Paul Scherrer Institute, 5232 Villigen, Switzerland.

Daniel Söderström is with the Department of Physics, University of Jyväskylä, 40014 Jyväskylä, Finland.

Arto Javanainen is with the Department of Physics, University of Jyväskylä, 40014 Jyväskylä, Finland, and also with the Electrical Engineering and Computer Science Department, Vanderbilt University, Nashville, TN 37235 USA.

Frédéric Saigné is with the Institute d' électronique et des systemès, Université de Montpellier, 34090 Montpellier, France.

Color versions of one or more figures in this article are available at https://doi.org/10.1109/TNS.2021.3070216.

Digital Object Identifier 10.1109/TNS.2021.3070216

I. Introduction

CHARGED pions are hadrons which, by inelastic interaction with the target nuclei, can release secondary ions capable of causing hazards as critical as single-event latch-up (SEL) in electronic devices. Although SEL hardening techniques exist [1], they are rarely applied in commercial static random access memories (SRAMs), which are typically characterized by very high heavy-ion cross sections [2] and can exhibit latch-up also in high-energy hadron (HEH) environments [3], [4].

An experimental study on pion single-event upset (SEU) and SEL cross sections was performed in [5]. For SEU, the pion cross-section shape directly reflected the typical reaction cross-section resonance in silicon in the 75–250 MeV energy region [6]. However, for SEL, the measured pion cross-section enhancement was not limited to the established resonance region, but extended at lower energies without any straightforward explanation.

While there are at least a few articles in the literature [7], [8] dealing with pion cross section measurements, and one [5] directly dealing with their impact in an accelerator environment, all these studies focused on SEUs. SEL rate predictions in the accelerator environment were shown to be quite a concern for certain memories characterized by strong energy dependence in the proton cross section [9], [10]. This was shown to be caused by the fragments released by the primary particles interacting with the tungsten layers nearby the sensitive volume (SV) of the device [11], [12]. The effect was very relevant at energies above the typical 200-MeV proton energy, used as a reference for testing and extended up to 3 GeV.

For typical accelerator environments, the pion fluxes peak at 1 GeV [13]. For the SEU case [5], it was concluded that the effect on the soft error rate (SER) was limited because the pion resonance was not extending beyond 250 MeV. However, this conclusion has to be verified for SELs in order to confirm that their rates in the accelerator are not underestimated.

Furthermore, the HEH equivalence approximation [14] neglects the impact of charged hadrons at energies below 20 MeV. There is no experimental indication that the pion

TABLE I
LIST OF TESTED DEVICES AND THEIR FEATURES

Manufacturer	Reference	Datecode	Technology
Brilliance	BS62LV1600EIP55	9254	180 nm
Lyontek	LY62W20488ML	1529	180 nm

SEL cross section would reduce similar to that of protons around and below this energy. Hence, this may provide a further source of inaccuracy.

This work delves, in more detail, into the nuclear mechanisms with the aim of understanding what stands behind the experimentally observed enhancement of the pion SEL cross section with respect to that of protons. In order to achieve this, this work strongly relies on the numerical analysis of SEL cross-section responses as well as on the study of basic pion–silicon and proton–silicon nuclear interactions. The obtained simulation benchmarks are also used to calculate the SEL rate expected in mixed-field environments and to assess the consequences of the extended pion SEL cross-section enhancement on the HEH equivalence.

II. EXPERIMENTAL INVESTIGATION

SRAMs are extensively used in the CERN Large Hadron Collider (LHC) complex for radiation detection purposes [15] as well as in the equipment exposed to the harsh radiation environment [16]. In the former case, components having a rather weak radiation tolerance are a better fit, whereas in the latter, harder devices are more suited. Nevertheless, in both cases, the pion SEL cross-section enhancement may have a negative impact. On the one hand, by overpredicting the hadronic flux, and, on the other hand, by underestimating the rate of power cycles in the electronic equipment, which would result in an availability underperformance for fundamental physics experiments.

The pion experimental tests have been performed at the Paul Scherrer Institute (PSI), at the piM1 facility. The facility and the flux calibration are extensively described in [5] and [17]. Currently, the facility cannot provide pion fluxes well suited for extensive SEL testing. This limited the number of devices for which a statistically significant amount of events at various energies could be collected in reasonable time.

Information on the tested references is reported in Table I. The rather high cross section of the two tested references allowed covering the whole available energy range at the facility (51–233 MeV).

The high-energy proton SEL measurements were performed at Kernfysisch Versneller Instituut (KVI) [18] in an energy range of 50–186 MeV and at PSI [19] for 30 and 230 MeV. The data acquisition procedure was the same as for the pions.

During the tests, the SRAMs were biased at 3.3 V, irradiated with the package on and at room temperature. One device per reference was tested with both pions and protons. The input current was monitored with a Keysight E3648A, whose maximum current was set to 0.5 A in order to protect the devices under test (DUTs). The nominal current of these memories is typically below 1 mA. A latch-up was recorded

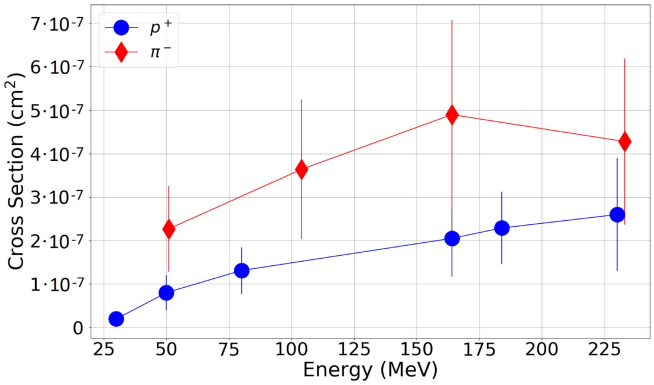

Fig. 1. Negative pion and proton SEL cross sections for the Brilliance SRAM with 95% confidence level error bars [5].

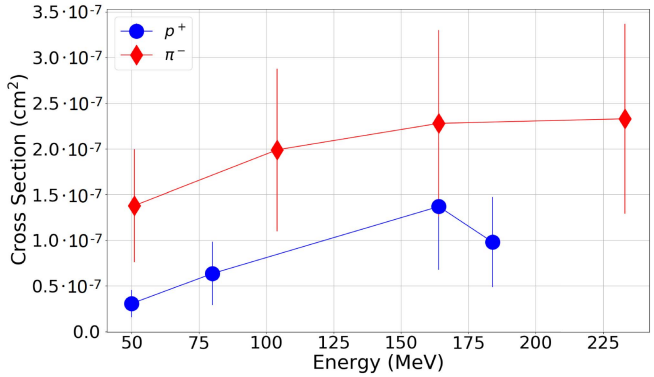

Fig. 2. Negative pion and proton SEL cross sections for the Lyontek SRAM with 95% confidence level error bars [5].

whenever the input current increased above 10 mA. In order for the event to be counted as an SEL, the high-current state was kept for 600 ms. Then, the equipment automatically cut the supply to the memory for 900 ms in order to remove the high-current state. Typically, the observed high-current states were between 300 and 500 mA for both devices, regardless of the primary particle or its energy. The tests were stopped whenever about 100 SELs were detected for each tested particle and energy. The devices did not experience any power consumption increase during the test. However, they were not tested after irradiation to check whether read/write operations had been affected.

The experimental data are reported with error bars with 95% confidence level. For both the pion and the proton error bars, an uncertainty on the fluence of $\pm 10\%$ is considered. For piM1, the uncertainty on the fluence has been verified by using different sets of instruments based on scintillators and ionization chambers, and time-of-flight measurements have been performed to determine the pion contribution to the overall flux [5].

Fig. 1 reports the SEL cross section of the Brilliance SRAM as a function of the tested energies for both pions and protons. The pion SEL cross section is a factor of 2–2.5 higher than that of protons for the entire tested energy range.

Fig. 2 shows the SEL cross section of the Lyontek SRAM as a function of the tested energies for both pions and protons.

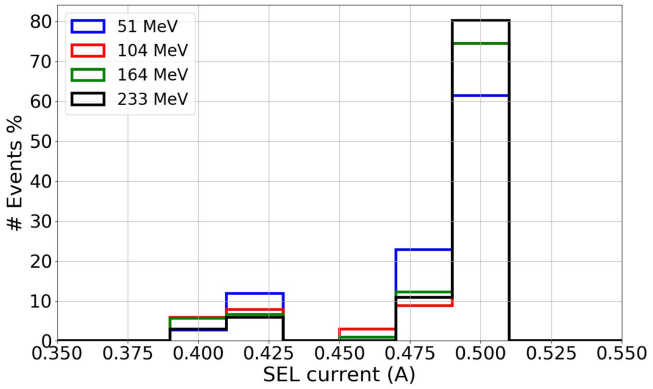

Fig. 3. Histograms of the distribution of high-state currents due to pion interactions of the tested energies for the Brilliance SRAM. The red bin is underneath the green bin for 0.5 A.

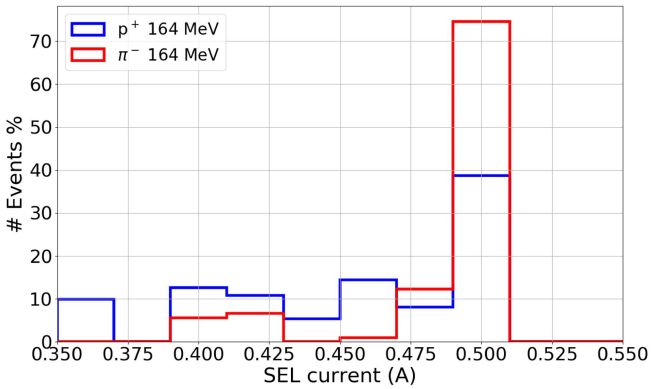

Fig. 4. Histograms of the distribution of high-state currents due to pion and proton interaction at a primary energy of 164 MeV for the Brilliance SRAM.

In this case, the pion SEL cross section is more than a factor of 3 higher at 50 MeV and is generally up to a factor of 2 higher for the other energies.

Fig. 3 reports the histogram of high-current states of the Brilliance SRAM for all the tested pion energies. Although the current consumption was limited to 0.5 A to preserve the integrity of the SRAM, the intensity distribution of the high-current state is not seen to vary much with the pion energy.

Fig. 4 depicts the same histogram, but this time comparing pion and proton high-current states at the same energy of 164 MeV. Note that the pion high-current states concentrate toward the upper limit, whereas proton high-current states are much more distributed. This is relevant for reliability in the accelerator mixed field, given that pions are not only expected to trigger a larger fraction of the total SEL count, but also to develop higher current states than protons.

III. Modeling and Monte Carlo Simulations of Pion SEL Cross Sections

An integral rectangular parallelepiped (IRPP) model can be used to replicate the SV of the device and determine the energy deposition events contributing to the SEL response. The heavy-ion SEL cross section as a function of linear energy transfer (LET) (described in terms of its Weibull function [20]) is convolved with the energy deposition distribution probability (converted to volume-equivalent LET through division by the SV thickness and the silicon density), produced by secondary ions of protons or pions, to retrieve the numerical SEL cross section from a beam of protons or pions. For the Brilliance SRAM, the heavy-ion Weibull fitting parameters are: $\sigma_{\text{sat}} = 0.6$ cm^2, $\text{LET}_0 = 2.4$ MeV/(mg/cm^2), $W = 13.7$ MeV/(mg/cm^2), and $s = 1.8$. However, they are not known for the Lyontek SRAM. Hence, the following analysis focuses on the Brilliance SRAM.

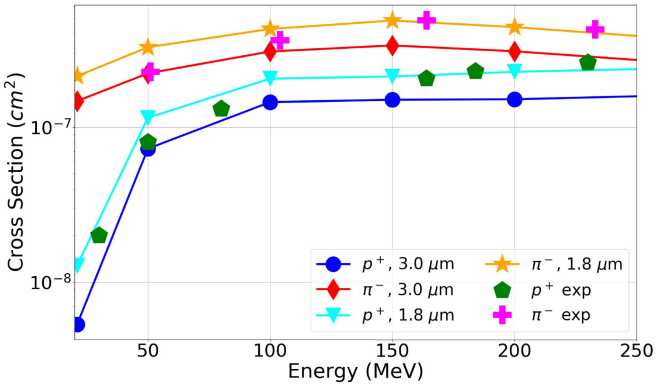

Fig. 5. Proton and negative pion SEL cross sections simulated with FLUKA for an SV thickness of 3.0 and 1.8 μm and compared to the Brilliance experimental data.

The sensitive size for the memory in the model was derived from the observations on SEL induction regions achieved on SRAM structures of 180 nm [21] performed with laser testing, which was proved to provide reliable results for protons and neutrons [9]. Laser testing was shown to be a valuable complementary tool in the qualification process of integrated circuits as it can enable determining the characteristics of the SV such as the size [21], [22], and the thickness [23] as well as to correlate it with the heavy-ion response for determining the LET threshold [24], and the cross section [25] or even the number of sensitive cells within the device [26]. All this information can be used to retrieve a better estimation of expected SEL rates in application.

A surface of 20×4 μm^2, representative of an array of 10×2 cells, is then used. Other than this, the simulations employ a 6-μm silicon back-end-of-line (BEOL) and a tungsten overlayer 0.4 μm thick. The thickness of the SV is kept as the free parameter for fitting the energy deposition events into an actual SEL hadron cross section. An SV thickness between 1.8 and 3 μm can fairly represent the SRAM SEL response and is compatible with thicknesses proposed for similar models in SRAMs manufactured in 180-nm technology [27]. It is also in good agreement with the observation that SEL structures in SRAMs are usually wider and longer rather than thicker [28].

Fig. 5 presents the FLUKA 4.0 [29], [30] simulation data for two thicknesses and the two particles compared to experimental data. No perfect thickness matching for both the lower (<100 MeV) and higher (>100 MeV) energy part of the cross-section curves was found.

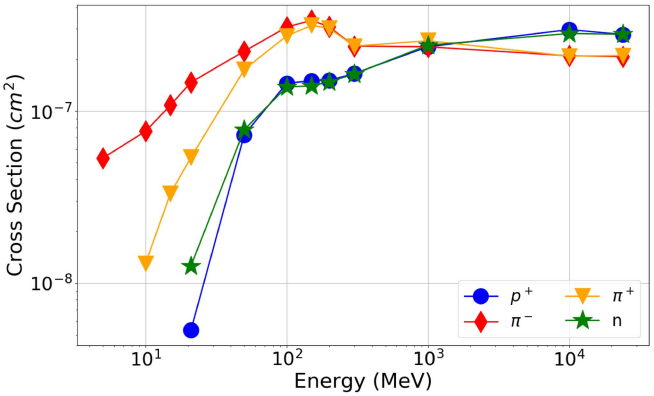

Fig. 6. FLUKA-simulated SEL cross sections as a function of energy for protons, charged pions, and neutrons. The energy range is meant to cover that of the CHARM facility.

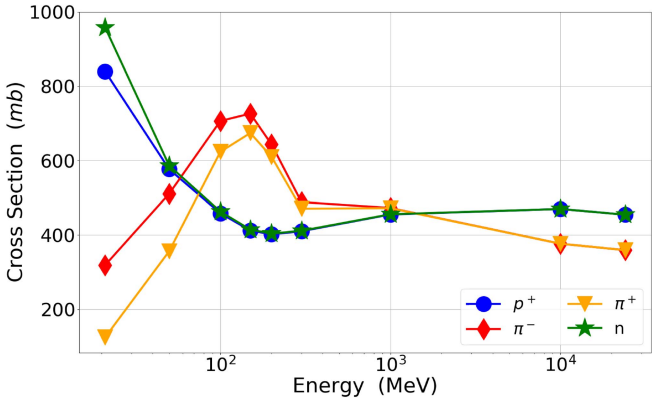

Fig. 7. Nuclear reaction cross section in millibarns (1 mb = 10^{-27} cm^2) of protons, neutrons, negative pions, and positive pions when interacting with silicon nuclei as a function of energy. For pions, this includes inelastic scattering and absorption.

The largest thickness was found to better describe the lower energy part, whereas the smallest was found to better replicate the higher energy part. These observations apply to both protons and negative pions. The disagreement between the models is small, that is, the model based on the smaller thickness returns, on average, cross sections which are 33% higher than those from the model with the larger thickness.

The larger thickness model is taken as a baseline, which will be verified in the nuclear interaction mechanisms and used for the accelerator radiation hardness assurance (RHA) considerations.

SEL cross sections are simulated for other particles making up the accelerator mixed-field, that is, positive pions and neutrons and for an extended range of energies meant to cover the whole spectra of spallation products typically found in the accelerator environment. Those cross sections are reported in Fig. 6. No significant differences are found between protons and neutrons all along the energy range (except at 21 MeV). On the other hand, the pion cross sections are always higher than those from the other two hadrons starting from well below 20 MeV up to 1 GeV, where the pion, proton, and neutron SEL cross section finally match.

Note that while the proton and neutron cross sections fade by more than one order of magnitude at 20 MeV with respect to their high-energy value, the negative pion cross section remains as high as the 50-MeV proton cross section even down to 5 MeV.

In the HEH approximation, the cross section of all hadrons is taken to be a step function starting at 20 MeV and equal to the proton cross section at 200 MeV. This would be quite conservative when considering protons and neutrons due to the observed fallout. However, ignoring the fact that pions can induce SEL even at energies below 20 MeV may lead to underestimations of the expected SEL cross section in mixed fields, although the presence of packaging may compensate for that.

The other interesting observation is that, while positive pions have the same charge as protons, their SEL cross section is about ten times higher at 21 MeV than that of protons and fades by one order of magnitude with respect to high energies only at 10 MeV.

IV. Nuclear Interaction Mechanisms Behind the Observed Enhancements

A. Nuclear Reaction Cross Section

One of the main parameters that can affect the SEL cross section response of pions with respect to protons is the nuclear reaction cross section. This is the probability that a pion or a proton of a certain energy will interact by either elastic or inelastic scattering with a silicon nucleus.

Fig. 7 reports the nuclear reaction cross sections of protons, neutrons, and charged pions in silicon as a function of the primary energy. Protons and pions exhibit very contrasting behaviors when it comes to their primary energy. At 200 MeV, both negative pions and positive pions have a reaction cross section which is at least 50% higher than that of protons. At 21 MeV, the situation is reversed with protons now having a cross section more than twice as high as that at 200 MeV, whereas the negative pion reaction cross section halves and the positive pion reaction cross section is four times lower than at 200 MeV. As a result, the proton reaction cross section is about a factor of 2.5 higher than that of negative pions and a factor of 7 higher than that of positive pions.

Higher probability of interaction means higher yield of secondary ions capable of depositing a sufficiently high amount of energy to trigger a single-event effect (SEE) at the same primary particle fluence. What the reaction cross section by itself does not say is how many secondary particles are released due to the nuclear interaction and which are their properties.

B. Scoring of Secondary Ions by Atomic Number

The preex tool available in FLUKA allows resolving all the possible nuclear interactions between primary particles and target nuclei on a statistical basis. The underlying physics is based on preequilibrium and evaporation models. The physics models for pion nuclear interaction in FLUKA are described in detail in [31]–[33]. Preex allows the extrapolation of distributions of byproducts in terms of species, kinetic energy, LET, and range. The numerical simulations are performed by

TABLE II

AVERAGE NUMBER OF REACTION PRODUCTS RELEASED BY PROTON, NEGATIVE PION, AND POSITIVE PION INTERACTIONS WITH SILICON NUCLEI FOR UNIT NUCLEAR REACTION

Primary energy [MeV]	By-products p^+-Si	By-products π^--Si	By-products π^+-Si
21	2.60	5.17	4.95
200	5.11	6.13	6.10

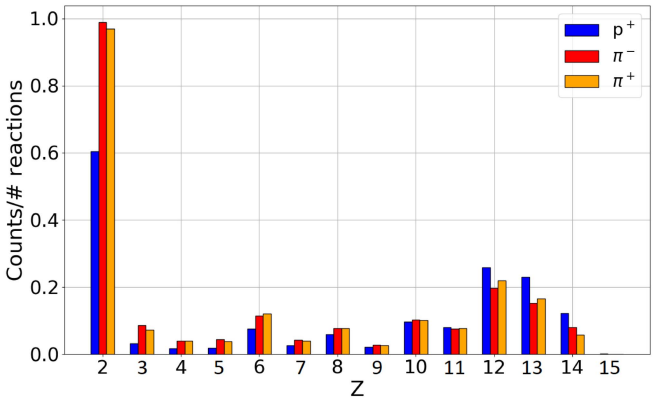

Fig. 8. Yield of secondary ions produced by nuclear reactions as a function of their atomic number normalized to the number of interactions for mono-energetic protons, negative pions, and positive pions at 200 MeV.

forcing the interaction of one million primary particles with one million silicon nuclei. Natural silicon is used as a target material. Hence, its isotopic composition is: 92.23% of ^{28}Si, 4.67% of ^{29}Si, and 3.10% of ^{30}Si.

Table II reports the average number of reaction products produced by forcing the nuclear interaction of one million primaries with the silicon nuclei as a function of the primary particle and its energy. This is used to extract more detailed scoring than what it is obtained from the Monte Carlo (MC) simulations (for which biasing was used to enhance the nuclear reaction cross section as otherwise only one in a few hundreds of thousands of primaries would have an interaction with a silicon nucleus).

Note that the minimum number of reaction products for each nuclear reaction is 2, for which the products would be the original primary particle and the Si nucleus after having exchanged momentum. Clearly, the value of 2.6 for 21-MeV protons indicates that it is quite common for protons of this energy, and the nuclei they interact with, to simply experience an exchange of momentum. Both charged pions at 21 MeV release on average five reaction products.

The situation is more homogeneous among protons and pions at 200 MeV, with protons releasing up to five reaction products and pions up to six, on average.

Figs. 8 and 9 propose the comparison of the yield of secondary ions released in proton–silicon and pion–silicon nuclear interactions at 200 and 21 MeV, respectively. The ions are identified by their atomic number and the yield is normalized by the one million simulated reactions.

There are not many differences at 200 MeV among the secondary ions released by proton–silicon and pion–silicon interactions. That is, similar reaction channels are open.

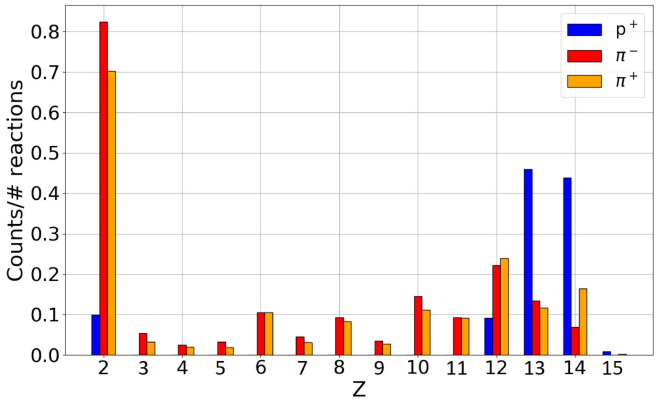

Fig. 9. Yield of secondary ions produced by nuclear reactions as a function of their atomic number normalized to the number of interactions for mono-energetic protons, negative pions, and positive pions at 21 MeV.

Note that pions seem to produce a larger amount of lighter ions (from $Z < 8$), which is quite evident for alphas. On the other hand, protons release a slightly higher amount of heavier ions ($Z > 11$). This indicates that protons are more likely to just knock a proton, a neutron or an alpha particle out of the nucleus, turning the latter into an aluminum ion, a silicon ion (different isotope) or a magnesium ion, respectively. On the other hand, pions are likely to induce a higher level of fragmentation, yielding also ions with intermediate Z between alphas and magnesium.

Such effects become even more evident when considering a primary energy of 21 MeV. At this energy, all the proton–silicon interactions seem to belong to a handful of reactions. On the other hand, for pions, basically all the reaction channels that were open at 200 MeV are still open at 21 MeV. As a result, both lighter and heavier ions are produced in similar quantities to the 200-MeV case.

For the 200-MeV case, when considering both the amount of reaction products and the relative nuclear reaction cross section (which was about 50% higher for the pions), one can conclude that the number of reaction products produced by the same number of primary protons and pions would be, when normalized to a single proton interaction, about 5 for the protons and about 9 for the pions. As a result, the number of secondary ions generated by pions will be about twice those released by protons, yielding the factor of 2 difference observed in the SEL cross section response at 200 MeV.

At 21 MeV, the positive and negative pions have rather similar average amounts of reaction products. However, when combined with the respective nuclear reaction cross sections, the negative pions would yield twice as many secondary ions as the positive pions. This is reflected in the simulated positive pion SEL cross section, which is about half that of negative pions at 21 MeV.

Note that the combination of the average number of reaction products and the nuclear reaction cross section alone is not enough to describe the enhanced pion cross section at 21 MeV with respect to that of protons. Hence, analyzing other properties of the secondary ions, such as their kinetic energy, LET, and range may help shed light on this difference.

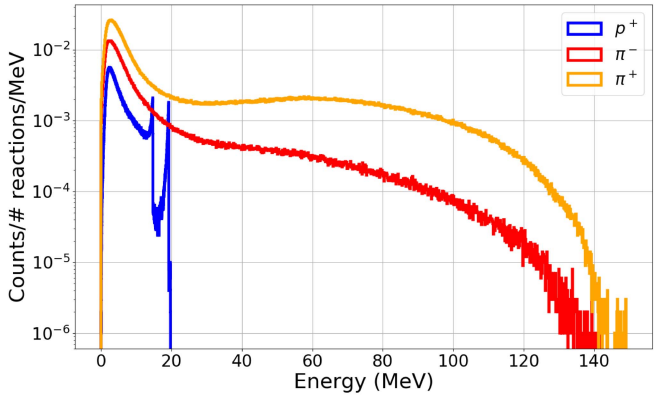

Fig. 10. Yield of secondary protons normalized to the number of interactions as a function of their kinetic energy for mono-energetic protons, negative pions, and positive pions at 21 MeV.

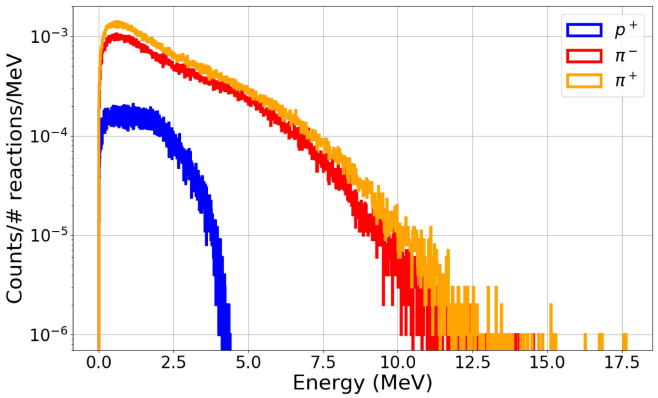

Fig. 11. Yield of secondary Mg ions normalized to the number of interactions as a function of their kinetic energy for mono-energetic protons, negative pions, and positive pions at 21 MeV.

C. Pion Absorption Impact on Secondary-Ion Kinetic Energy

In spite of their common hadronic nature, pions interact differently with heavy nuclei than protons. One of the main mechanisms in pion–silicon interactions, regardless of the charge of the pion, is the pion absorption (which can contribute to more than 50% of the total nuclear reaction cross section for positive pions and up to 70% for negative pions [34]). This results in the emission of a few additional secondary particles. The main peculiarity of these secondary particles is that, even at low primary energy of the incident pion, they may be emitted with quite high kinetic energy.

One example of the consequences of the pion absorption on the kinetic energy of secondary particles is shown in Fig. 10. The yield of secondary protons emitted by proton–silicon and pion–silicon interactions as a function of their energy is shown for a primary particle energy of 21 MeV. Note that the protons emitted have a hard limit in the energy which corresponds to the energy of the primary. On the other hand, the secondary protons emitted by pion–silicon interactions have a continuous distribution in energy up to about 140 MeV. This behavior is known from past experimental measurements [35]. Basically, when absorbed, a pion can excite the nucleus to the point that highly exothermic reactions are triggered, releasing secondary particles with high kinetic content.

Fig. 11 reports the yield of magnesium ions released by proton–silicon and pion–silicon interactions as a function of their energy for a primary particle energy of 21 MeV. The same behavior observed for protons occurs for ions of any atomic number. However, the kinetic energy transferred to ions of growing atomic mass is lower. For magnesium, pions can provide up to 13 MeV of kinetic energy, whereas protons can only provide up to 4 MeV.

As shown, thanks to this absorption mechanism, pions are capable of emitting a spectrum of secondary ions which are more than twice as energetic as those emitted by protons.

The pion absorption cross section provides a nonnegligible contribution to the nuclear reaction cross section (Fig. 7) at any energy. However, its effects on the secondary ion characteristics do not scale up with energy because the kinetic content available to the secondary ions is always coming from the pion rest mass (139 MeV/c^2), which is fixed. This can be appreciated in Fig. 12, which depicts the yield of secondary protons from 200-MeV primaries.

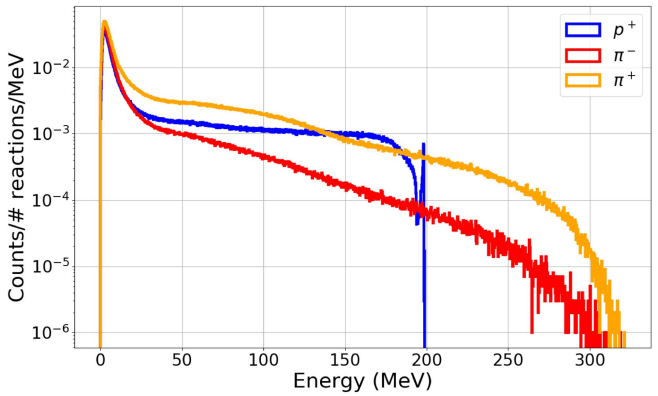

Fig. 12. Yield of secondary protons normalized to the number of interactions as a function of their kinetic energy for mono-energetic protons, negative pions, and positive pions at 200 MeV.

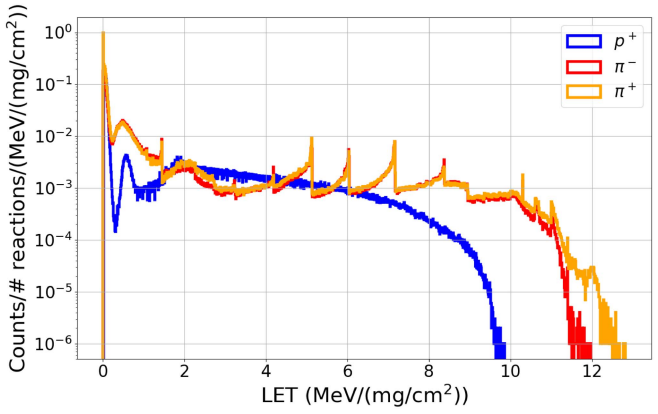

Fig. 13. Yield of secondary ions normalized to the number of interactions as a function of their LET for mono-energetic protons, negative pions, and positive pions at 21 MeV.

D. LET and Range of Secondary Ions

Fig. 13 shows the yield of secondary ions as a function of their LET upon generation normalized to the number of

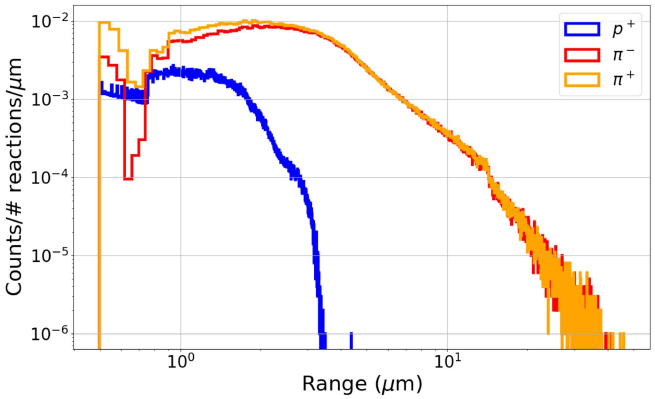

Fig. 14. Yield of secondary ions normalized to the number of interactions as a function of their range for mono-energetic protons, negative pions, and positive pions at 21 MeV.

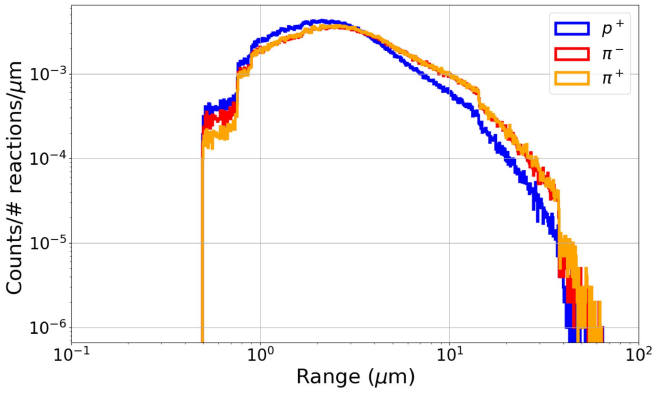

Fig. 15. Yield of secondary ions normalized to the number of interactions as a function of their range for mono-energetic protons, negative pions, and positive pions at 200 MeV.

interactions for protons, negative pions, and positive pions at 21 MeV. When considering LET, the atomic number of the ion is disregarded, assuming that all ions of similar LET will behave similarly.

No big differences are seen between negative and positive pions. On the other hand, the proton LET distribution is much different as it is missing the discrete peaks. This is due to the lack of secondary ions with intermediate and low Z (<12). On the other hand, magnesium, aluminum, and silicon ions are produced in a rather wide range of energies that lead to a quite smooth LET distribution.

Although having quite distinct shapes, proton and pion LET distributions do not seem to indicate that the SEL cross section for protons would be that much lower than those of charged pions. Indeed, these distributions will have to be scaled by the nuclear reaction cross section, which, at this energy, is higher for protons.

The range of secondary ions is an important parameter. For instance, it was shown that the range distribution of secondary ions can explain the angular dependence of proton and neutron SEL cross sections in SRAMs [3].

Fig. 14 reports the yield of secondary ions as a function of their range normalized to the number of reactions for protons, negative pions, and positive pions at 21 MeV. Note that the plot does not include all secondary ions. Ions with LET upon generation below 2.4 MeV/(mg/cm^2) have been filtered out since this is the heavy-ion LET threshold of the Brilliance SRAM.

With the imposed filtering based on the ion LET threshold, all secondary ions have range above 500 nm for both proton and pion distributions.

The range distributions are very different for proton and pion secondary ions. All secondary ions from proton–silicon interactions and a sufficiently high LET have ranges below 3.5 μm. On the other hand, the pion–silicon interactions can release ions with range as high as 40 μm. The pion distributions are also seen to peak just above 3.5 μm, where the proton distribution fades.

Fig. 15 depicts the yield of secondary ions as a function of their range normalized to the number of reactions for protons, negative pions, and positive pions at 200 MeV. At this energy, protons and pions generate secondary ions with very similar range distributions. Therefore, considering that pions yield twice as many secondaries as protons at 200 MeV, it is confirmed that the nuclear reaction rate alone is enough to explain the SEL cross section increase of a factor of 2 observed experimentally.

E. LET Equivalent as Key Metric

Different from SELs, SEUs can develop even when a quite low charge is collected in the SV. This is the reason why in small SVs associated with SEUs, not only secondary ions, but also direct ionization from protons can cause upsets [36]. On the other hand, the range distribution of ions, taken in relative terms with respect to the SV thickness, is a decisive parameter when it comes to SEL triggering [37], [38]. In this case, the LET of the secondary ions is not a good metric to determine the hadron response [39], [40] because most of the secondary ions will not have a range long enough to transverse a significant portion of the SV and deposit enough energy to trigger an SEL.

In such context, a different metric has to be used, that is, the volume equivalent LET ($\mathrm{LET_{EQ}}$) [39], [41]. This metric can be used to perform a new scoring of the secondary ion distributions from protons and pions when the range R of the secondary ion is shorter than the SV thickness, as indicated below:

$$\begin{cases} \mathrm{LET_{EQ}} = \dfrac{E_k}{\rho t} & R \leq t \\ \mathrm{LET_{EQ}} = \mathrm{LET} & R > t. \end{cases} \tag{1}$$

Here, E_k is the kinetic energy of the secondary ion upon generation, ρ is the density of the material where the energy deposition occurs (in this case silicon), and t is the thickness of the SV. Hence, this metric classifies the secondary ions depending on the properties of the SV. In accordance with the SV proposed for the MC simulations, the thickness is taken to be 3 μm.

Note that when an ion has a range long enough to go through the whole SV thickness and beyond, its $\mathrm{LET_{EQ}}$ is assumed to be equal to the LET upon generation.

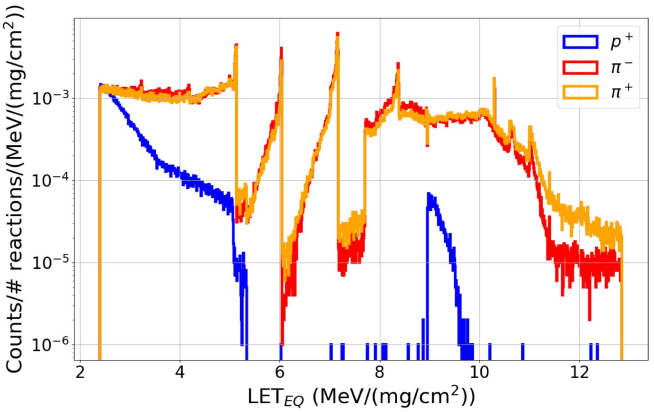

Fig. 16. Yield of secondary ions normalized to the number of interactions as a function of their LET_{EQ} for mono-energetic protons, negative pions, and positive pions at 21 MeV.

TABLE III

SEL Cross Sections Calculated by Convolving the Heavy-Ion Weibull Curve With the LET Spectra of Fig. 13 and With the LET_{EQ} Spectra of Fig. 16. The SEL Cross Sections Obtained From the MC Simulations for Protons and Charged Pions Are Also Reported. The SEL Cross Section Units Are cm^2/Dev

Method	σ SEL protons	σ SEL negative pions	σ SEL positive pions
LET	$2.96 \cdot 10^{-7}$	$3.36 \cdot 10^{-7}$	$1.32 \cdot 10^{-7}$
LET_{EQ}	$9.90 \cdot 10^{-9}$	$2.27 \cdot 10^{-7}$	$8.99 \cdot 10^{-8}$
Monte-Carlo	$5.34 \cdot 10^{-9}$	$1.47 \cdot 10^{-7}$	$5.38 \cdot 10^{-8}$

Fig. 16 reports the yield of secondary ions as a function of LET_{EQ} normalized to the number of interactions for protons and pions at 21 MeV. As done for the range, the plot reports only the secondary ions having an LET_{EQ} above 2.4 MeV/(mg/cm^2).

The pion distributions in terms of LET_{EQ} have preserved somewhat the shape that was shown in the LET-upon-generation distributions in Fig. 13. Indeed, there are still particles having LET as high as 12 MeV/(mg/cm^2), though in lower abundance. The biggest difference is the deeper lowering on the left side of each peak, which shows that secondary ions generated with LET in defect of that at the peak are often associated with a range shorter than the SV thickness.

The differences between the proton LET and LET_{EQ} distributions are much more evident. The previous continuous distribution is now replaced by a first continuous distribution fading at an LET_{EQ} just above 5 MeV/(mg/cm^2) and a secondary peak at LET_{EQ} of 9–10 MeV/(mg/cm^2). The latter represents the residual amount of magnesium, aluminum, and silicon ions having a long enough range.

The LET_{EQ} distributions represent a more faithful picture of what is happening inside the SV. As a cross-check, the heavy-ion Weibull curve, which is used in the MC IRPP method to calculate the cross section response, can be convolved along with the spectra reported in Fig. 16 and multiplied by the respective nuclear reaction rates to get an SEL cross section.

Table III reports the SEL cross sections determined with this method for the LET distributions and for the LET_{EQ} distributions for the three primary particles as well as the SEL cross sections obtained from the MC simulations. When convolving with the pure LET spectra, the proton SEL cross section is predicted to be as high as that of negative pions. However, when using the LET_{EQ} spectra, both the proton and the pion SEL cross sections are much closer to those calculated through a full transport MC analysis.

The residual differences between the LET_{EQ} spectra and the MC simulations is due to the fact that the angular distribution of the emitted secondary ions is neglected in the LET_{EQ} calculation. Hence, secondary ions may have, within the SV, ionization tracks longer or shorter than the SV thickness.

In addition, the LET_{EQ} calculation takes all ions as emitted at the top surface of the SV, whereas in the MC simulations, the events generating secondary ions can occur at any point inside or outside the SV and the relative distance to the SV edge can play a role on whether an ion will deposit sufficient energy to trigger an SEL or not.

TABLE IV

Hadronic Abundance of Hadrons for Some Test Positions Inside CHARM [13]. All Charged Pions Are Grouped Together. Proton, Neutron, and Kaon Fluxes Are Integrated Above 20 MeV, Pion Fluxes Above 1 MeV

Position	Pions	Protons	Neutrons	Kaons
R5	15.9%	13.8%	69.8%	0.6%
R10	22.8%	17.3%	58.8%	1.1%
R13	37.1%	20.2%	42.8%	0.0%

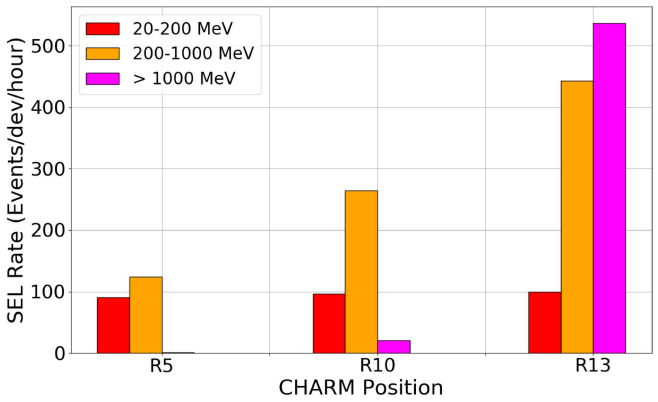

Fig. 17. SEL rates from pions from three energy ranges and three CHARM positions.

V. RHA Implications

The CERN Highly-AcceleRated Mixed-field facility (CHARM) facility [42] is taken as a study case for the RHA considerations given its wide representativeness of the various mixed-field radiation environments at CERN. The fluxes used for the computations have been calculated by means of FLUKA simulations of the facility [13]. Table IV reports the hadronic abundance in percentage of all hadrons generated in mixed fields. The pion contribution to the total flux can be as low as 16% for the R5 test position in the CHARM facility and as high as 37% for the R13 position.

Fig. 17 depicts the pion SEL rate contributions for various CHARM positions by subdividing their contributions

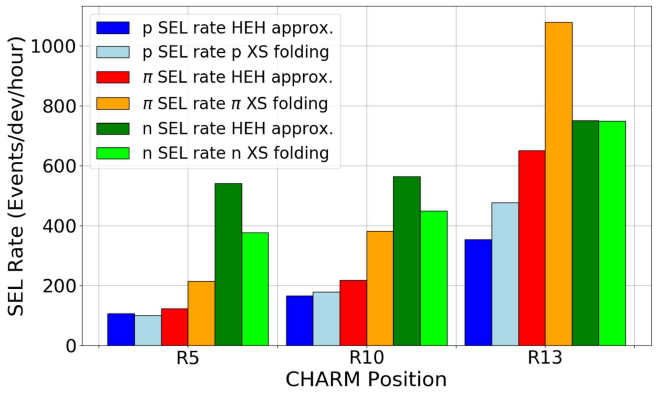

Fig. 18. SEL rate comparison between the HEH approximation approach and the full particle folding approach (XS = cross section). Data are reported by CHARM position and further subdivided for protons (blue), pions (red), and neutrons (green).

into three energy ranges: 20–200 MeV, 200–1000 MeV, and >1 GeV. As the plot shows, contributions to the total pion SEL rate may vary widely depending on the position. Typically, the 200–1000 MeV pion fluxes provide a higher contribution than the 20–200 MeV pion fluxes to the total SEL rate by up to a factor of 4. Pion fluxes with energy >1 GeV are an important contributor only for position R13, given that they are 15 times and 200 times higher than in R10 and R5, respectively.

The HEH approximation in mixed field for the calculation of the SEL rate is based on the assumption that all particles have the same exact response regardless of their nature and energy. In addition, that response would be equal to a step function starting at 20 MeV and with the proton cross section at 200 MeV as step value. The actual SEL response in mixed field can more precisely be calculated by convolution of each particle spectrum with the respective SEL cross section as a function of energy. For this purpose, the numerical SEL cross sections shown in Fig. 6 are used since they allow covering a wider range of energies than the experimental cross sections.

Fig. 18 shows the contribution of each particle to the total SEL rate (positive and negative pion contributions are shown together) for three CHARM characteristic test positions representative of the low-Earth orbit trapped proton (R5), accelerator- and atmospheric-like (R10) and accelerator highly energetic (R13) environments, respectively.

For all the three environments, the pion contribution to the total SEL rate is underestimated when using the HEH approximation by factors of 1.6–2, depending on the pion abundance. For protons and neutrons, the HEH approximation provides either a fair or a conservative estimation. For the total SEL rate, while underestimating the pion contribution, the HEH approximation provides a fair estimation for R5 and R10, being the ratios between the actual fluxes SEL rate and that delivered by the HEH approximation equal to 0.87 and 1.07, respectively. For the R13 position, the underestimation from the HEH approximation is stronger, since this ratio is 1.43.

Following these results, the HEH approximation still provides valuable estimations of the device SEL response in mixed fields in most of the application cases. Hence, characterizing the SEL cross section out of the single 200-MeV proton datapoint remains a valuable qualification scheme for accelerator applications. At the same time, the SEL rate predicted by experimental testing at CHARM and determined through the HEH approximation for other environments will be a fair representation of that obtained by proton testing.

For the only exception (R13), which concerns a small amount of accelerator equipment, the underestimation obtained by the single 200-MeV proton testing can be accounted for by assuming a margin of less than 50% on the predicted rate obtained through the HEH approximation.

VI. Conclusion

A pion SEL cross-section enhancement was experimentally observed on two SRAMs for the whole energy range under test. The enhancement was confirmed through MC simulations of the SV energy deposition responses based on an IRPP model.

Different from SEU, the pion SEL cross section was found to be higher than those of protons and neutrons for a wider range of energies. For the high-energy region (>100 MeV), it was shown that the factor of 2 higher pion cross section is due to the higher probability of pion interaction with silicon nuclei, that is, to the nuclear reaction cross section. At such energies, proton–silicon and pion–silicon reactions and their secondary products do not differ that much.

At lower energies (<100 MeV) and, in particular, for the 21-MeV case, it was shown that the nuclear reaction cross section alone cannot explain the observed enhancement, as it would lead to a similar SEL cross section for protons and pions. Secondary products were studied in terms of their main characteristics, such as kinetic energy, LET, and range. However, it was only when the SV dimensions were added to the context and the $\mathrm{LET_{EQ}}$ was introduced that the higher pion SEL cross section could be explained. The observed differences can be related to the higher energy provided to secondary products by the pion absorption mechanism, which occurs for both positive and negative pions.

Finally, the HEH approximation for mixed fields was tested against the pion SEL cross-section enhancement. The data for representative accelerator environments showed that the effect of the pion enhancement becomes significant only when pions are in larger amount. Even in those rare cases, a small margin on the SEL cross section measured with 200-MeV protons can be enough to account for the inaccuracy introduced by neglecting the pion cross-section enhancement.

References

[1] N. A. Dodds *et al.*, "Effectiveness of SEL hardening strategies and the latchup domino effect," *IEEE Trans. Nucl. Sci.*, vol. 59, no. 6, pp. 2642–2650, Dec. 2012.

[2] R. Harboe-Sorensen *et al.*, "The technology demonstration module on-board PROBA-II," *IEEE Trans. Nucl. Sci.*, vol. 58, no. 3, pp. 1001–1007, Jun. 2011.

[3] J. R. Schwank *et al.*, "Effects of angle of incidence on proton and neutron-induced single-event latchup," *IEEE Trans. Nucl. Sci.*, vol. 53, no. 6, pp. 3122–3131, Dec. 2006.

[4] R. Secondo *et al.*, "Analysis of SEL on commercial SRAM memories and mixed-field characterization of a latchup detection circuit for LEO space applications," *IEEE Trans. Nucl. Sci.*, vol. 64, no. 8, pp. 2107–2114, Aug. 2017.

[5] A. Coronetti *et al.*, "The pion single-event effect resonance and its impact in an accelerator environment," *IEEE Trans. Nucl. Sci.*, vol. 67, no. 7, pp. 1606–1613, Jul. 2020.

[6] H. H. K. Tang, "Nuclear physics of cosmic ray interaction with semiconductor materials: Particle-induced soft errors from a physicist's perspective," *IBM J. Res. Develop.*, vol. 40, no. 1, pp. 91–108, Jan. 1996.

[7] G. J. Hofman *et al.*, "Light-hadron induced SER and scaling relations for 16-and 64-Mb DRAMS," *IEEE Trans. Nucl. Sci.*, vol. 47, no. 2, pp. 403–407, Apr. 2000.

[8] S. Duzellier, D. Falguere, M. Tverskoy, E. Ivanov, R. Dufayel, and M.-C. Calvet, "SEU induced by pions in memories from different generations," *IEEE Trans. Nucl. Sci.*, vol. 48, no. 6, pp. 1960–1965, Dec. 2001.

[9] R. G. Alia *et al.*, "SEL cross section energy dependence impact on the high energy accelerator failure rate," *IEEE Trans. Nucl. Sci.*, vol. 61, no. 6, pp. 2936–2944, Dec. 2014.

[10] R. G. Alia *et al.*, "SEL hardness assurance in a mixed radiation field," *IEEE Trans. Nucl. Sci.*, vol. 62, no. 6, pp. 2555–2562, Dec. 2015.

[11] J. R. Schwank *et al.*, "Effects of particle energy on proton-induced single-event latchup," *IEEE Trans. Nucl. Sci.*, vol. 52, no. 6, pp. 2622–2629, Dec. 2005.

[12] R. G. Alia *et al.*, "Energy dependence of tungsten-dominated SEL cross sections," *IEEE Trans. Nucl. Sci.*, vol. 61, no. 5, pp. 2718–2725, Oct. 2014.

[13] A. Infantino, "FLUKA Monte Carlo modelling of the CHARM facility's test area: Update of the radiation field assessment," CERN, Geneva, Switzerland, Tech. Rep. CERN-ACC-NOTE-2017-0059, Nov. 2017.

[14] K. Roeed *et al.*, "Method for measuring mixed field radiation levels relevant for SEEs at the LHC," *IEEE Trans. Nucl. Sci.*, vol. 59, no. 4, pp. 1040–1047, Aug. 2012.

[15] G. Spiezia *et al.*, "A new RadMon version for the LHC and its injection lines," *IEEE Trans. Nucl. Sci.*, vol. 61, no. 6, pp. 3424–3431, Dec. 2014.

[16] S. Danzeca *et al.*, "Qualification and characterization of SRAM memories used as radiation sensors in the LHC," *IEEE Trans. Nucl. Sci.*, vol. 61, no. 6, pp. 3458–3465, Dec. 2014.

[17] W. Hajdas *et al.*, "High energy electron radiation exposure facility at PSI," *J. Appl. Math. Phys.*, vol. 2, no. 9, pp. 910–917, 2014.

[18] E. R. van der Graaf, R. W. Ostendorf, M.-J. van Goethem, H. H. Kiewiet, M. A. Hofstee, and S. Brandenburg, "AGORFIRM, the AGOR facility for irradiations of materials," in *Proc. Eur. Conf. Radiat. Effects Compon. Syst.*, Bruges, Belgium, Sep. 2009, pp. 451–454.

[19] W. Hajdas, F. Burri, C. Eggel, R. Harboe-Sorensen, and R. de Marino, "Radiation effects testing facilities in PSI during implementation of the proscan project," in *Proc. IEEE Radiat. Effects Data Workshop*, Phoenix, AZ, USA, Jul. 2002, pp. 160–164.

[20] E. L. Petersen, J. C. Pickel, J. H. Adams, and E. C. Smith, "Rate prediciton for single event effects," *IEEE Trans. Nucl. Sci.*, vol. 39, no. 6, pp. 1577–1599, Dec. 1992.

[21] N. A. Dodds *et al.*, "SEL-sensitive area mapping and the effects of reflection and diffraction from metal lines on laser SEE testing," *IEEE Trans. Nucl. Sci.*, vol. 60, no. 4, pp. 2550–2558, Aug. 2013.

[22] P. Wang *et al.*, "Analysis of TPA pulsed-laser-induced single-event latchup sensitive-area," *IEEE Trans. Nucl. Sci.*, vol. 65, no. 1, pp. 502–509, Jan. 2018.

[23] E. Faraud *et al.*, "Investigation on the SEL sensitive depth of an SRAM using linear and two-photon absorption laser testing," *IEEE Trans. Nucl. Sci.*, vol. 58, no. 6, pp. 2637–2643, Dec. 2011.

[24] A. J. Burnell, A. M. Chugg, and R. Harboe-Sørensen, "Laser SEL sensitivity mapping of SRAM cells," *IEEE Trans. Nucl. Sci.*, vol. 57, no. 4, pp. 1973–1977, Aug. 2010.

[25] V. Pouget, P. Fouillat, D. Lewis, H. Lapuyade, F. Darracq, and A. Touboul, "Laser cross section measurement for the evaluation of single-event effects in integrated circuits," *Microelectron. Rel.*, vol. 40, nos. 8–10, pp. 1371–1375, Aug. 2000.

[26] Y.-T. Yu, J.-W. Han, G.-Q. Feng, M.-H. Cai, and R. Chen, "Correction of single event latchup rate prediction using pulsed laser mapping test," *IEEE Trans. Nucl. Sci.*, vol. 62, no. 2, pp. 565–570, Apr. 2015.

[27] P. Wang *et al.*, "Sensitive-volume model of single-event latchup for a 180-nm SRAM test structure," *IEEE Trans. Nucl. Sci.*, vol. 67, no. 9, pp. 2015–2020, Sep. 2020.

[28] L. Artola *et al.*, "Analysis of angular dependence of single-event latchup sensitivity for heavy-ion irradiations of 0.18-μm CMOS technology," *IEEE Trans. Nucl. Sci.*, vol. 62, no. 6, pp. 2539–2546, Dec. 2015.

[29] G. Battistoni *et al.*, "Overview of the FLUKA code," *Ann. Nucl. Energy*, vol. 82, pp. 10–18, Aug. 2015.

[30] T. T. Böhlen *et al.*, "The FLUKA code: Developments and challenges for high energy and medical applications," *Nucl. Data Sheets*, vol. 120, pp. 211–214, Jun. 2014.

[31] A. Fassò, A. Ferrari, J. Ranft, and P. R. Sala, "FLUKA: Performances and applications in the intermediate energy range," in *Proc. 1st AEN/NEA Spec.' Meeting Shielding Aspects Accel., Targets Irradiation Facilities (SATIF)*, Arlington, TX, USA, Apr. 1995, pp. 287–304.

[32] A. Fassò, A. Ferrari, J. Ranft, and P. R. Sala, "An update about FLUKA," in *Proc. 2nd Workshop Simulating Accel. Radiat. Environ.*, Geneva, Switzerland, Oct. 1997, pp. 158–170.

[33] A. Ferrari, J. Ranft, S. Roesler, and P. R. Sala, "Cascade particles, nuclear evaporation, and residual nuclei in high energy hadron-nucleus interactions," *Zeitschrift für Physik C Particles Fields*, vol. 70, pp. 316–413, Jan. 1996.

[34] D. Ashery, I. Navon, G. Azuelos, H. K. Walter, H. J. Pfeiffer, and F. W. Schleputz, "True absorption and scattering of pions on nuclei," *Phys. Rev. C*, vol. 23, no. 5, pp. 2173–2185, May 1981.

[35] R. D. McKeown *et al.*, "Inclusive reactions of pions on nuclei," *Phys. Rev. C*, vol. 24, no. 1, pp. 211–220, Jul. 1981.

[36] A. Coronetti *et al.*, "Assessment of proton direct ionization for the radiation hardness assurance of deep sub-micron SRAMs used in space applications," *IEEE Trans. Nucl. Sci.*, early access, Feb. 22, 2021, doi: 10.1109/TNS.2021.3061209.

[37] A. H. Johnston and B. W. Hughlock, "Latchup in CMOS from single particles," *IEEE Trans. Nucl. Sci.*, vol. 37, no. 6, pp. 1886–1893, Dec. 1990.

[38] A. H. Johnston, "The influence of VLSI technology evolution on radiation-induced latchup in space systems," *IEEE Trans. Nucl. Sci.*, vol. 43, no. 2, pp. 505–521, Apr. 1996.

[39] R. Ladbury, J.-M. Lauenstein, and K. P. Hayes, "Use of proton SEE data as a proxy for bounding heavy-ion SEE susceptibility," *IEEE Trans. Nucl. Sci.*, vol. 62, no. 6, pp. 2505–2510, Dec. 2015.

[40] R. L. Ladbury and J.-M. Lauenstein, "Evaluating constraints on heavy-ion SEE susceptibility imposed by proton SEE testing and other mixed environments," *IEEE Trans. Nucl. Sci.*, vol. 64, no. 1, pp. 301–308, Jan. 2017.

[41] R. G. Alía *et al.*, "Simplified SEE sensitivity screening for COTS components in space," *IEEE Trans. Nucl. Sci.*, vol. 64, no. 2, pp. 882–890, Feb. 2017.

[42] J. Mekki *et al.*, "CHARM: A mixed field facility at CERN for radiation test in ground, atmospheric, space and accelerator representative environments," *IEEE Trans. Nucl. Sci.*, vol. 63, no. 4, pp. 2106–2114, Aug. 2016.